Assessing the effects of precursor material's carbon content on synthesized zeolites' properties: Applications in heavy metal adsorption

Stephen Majoni [1*], Tadini W. Masaya [2,3]

[1] *Department of Chemical and Forensic Sciences, Botswana International University of Science and Technology, Palapye, Botswana*
[2] *Department of Applied Chemistry, National University of Science and Technology, Bulawayo, Zimbabwe.*
[3]*Present address, Department of Chemistry, West Virginia University, Morgantown USA*

Abstract
Coal fired thermo-electric power stations generate large amounts of coal combustion by-products such as fly ash. The majority of the fly ash is currently being disposed of in ash dumps or landfills, with the associated environmental impacts. Zeolites synthesis is among several potentials uses of fly ash that have been investigated as a way to mitigate the environmental impacts of thermo-electric power stations. However, low boiler efficiencies may produce fly ash containing high amounts of unburnt carbon. We have evaluated the effects of high unburnt carbon content (20%, based on X-ray fluorescence analysis) on cation exchange capacities and adsorption properties of fly ash -based zeolites. Batch adsorption studies showed that the adsorption process followed the Langmuir adsorption isotherm. Non-linear and linear model fitting procedures conducted indicated that it is inappropriate to use linear forms of the kinetic expressions to determine the kinetics of the adsorption process. Despite lower adsorption capacities of zeolites made from high-carbon fly ash, they showed substantial Ca^{2+} ions adsorption activity.

1. Introduction

Fossil fuels make up a large portion of developing nations' electricity production, with coal having been projected to still cater for up to 35% of energy needs in Africa by 2025 [1, 2]. Globally, the consumption of coal for power generation is set to remain at 100 quadrillion Btu by 2050 [1]. Gaseous and particulate emissions from coal-fired thermoelectric power stations (cTPSs) are a major environmental concern. For example, on average each kWh of electric energy produced by cTPSs has an environmental impact in the order of 800 g of emitted carbon dioxide [3]. The coal combustion process generates solid residues commonly referred to as coal combustion by-products (CCPs) whose principal components are fly ash (FA), bottom ash (BA) and coal rubble/boiler slag (CR). Whereas FA is collected by electric precipitators, cyclones, or mechanical filters at the chimney flue of boilers, bottom ash and slag are collected from the bottom of the furnace. In general, cTPSs consuming 120-million tons of coal per annum for power generation generate about 25-million tons of ash made up of 60 to 88% FA [3].

The projected increase in coal consumption in Africa means thermal power stations are therefore faced with a problem of ash storage and disposal. In current practices, most power stations in Africa dispose ash in landfills or ash ponds. These disposal methods are not only costly in terms of land and the associated handling and transportation costs but are also environmentally unfriendly. FA disposed in landfills and ash ponds have been shown to leach heavy metals into the environment. The projected increase in CCPs generation will only exacerbate the problem as ash disposal competes with national developmental programmes requiring land. To minimize these effects, utilization of FA in various processes and industries has been widely investigated. FA has applications in a number of areas that include; catalysis, construction and ceramic industries [4–6], soil stabilization, zeolites and geopolymers synthesis [7–10], among other uses. The conversion of FA to zeolites is one of the most attractive approaches as zeolites have applications in diverse areas such as catalysis, ion exchange and adsorbent materials [11]. The synthesis of zeolites require sources of Si and Al, with commercial synthesis usually utilizing silica gel and Al salts in the presence of NaOH [12, 13]. CCPs, especially fly ash, are rich in silica and alumina which makes them good source materials for zeolite synthesis [11]. The chemical composition, and hence the properties of coal fly ash are greatly influenced by the type of the coal (formation and deposition) from which it was generated as well as the combustion conditions. However, it has been shown that the major constituents of FA are SiO_2 and Al_2O_3, with significant levels of CaO and Fe_2O_3, with some concentration variations depending on the class of source coal [14]. High levels of silica and alumina in FA have prompted continuous efforts on utilization of FA as source materials in zeolites synthesis [15–18]. In 1987, Henmi treated FA with NaOH and observed a substantial increase in the cation exchange capacity (CEC) that was attributed to formation of zeolites [19]. Since then, there has been keen interests in alkali activation of FA to produce zeolite [11, 20–22]. Fly ash containing high levels of unburnt carbon can originate from low operating furnace temperatures due to environmental regulations to mitigate NOx emissions, or boiler inefficiency due to old technologies and obsolete equipment [23]. High carbon content FA have low applicability due to the adverse effects of carbon in some applications such as concrete products [24]. There are a number of ways in which unburnt carbon can be separated/ removed from FA as a way of recovering carbon [23] or making FA more suitable for specific applications [25–29]. The current procedures in zeolite synthesis using FA as source materials entails pretreatment of the FA by calcination at high temperatures (800 to 1000 °C) to remove unburnt carbon [30]. This high energy process may become a cost barrier when the FA is consistently high in unburnt carbon due to old technologies in use in some developing countries. This work aims to evaluate the effects of high carbon content in source materials on the synthesis and properties of synthesized zeolites. The effect of unburnt carbon on CEC as well as on adsorption efficiency of synthesized zeolites will be assessed. Adsorption efficiency will be tested on the adsorption of Ca^{2+} ions to evaluate the applicability of the adsorbent on point of use water softening technologies, especially for communities that rely on borehole water. Adsorption isotherms and kinetics will be modelled by both linear and non-linear methods. Model fitting procedures will be conducted using both linear and non-linear methods to highlight the errors associated with linearization of models for curve fitting. The coefficient of determination (r^2), equation (1), will used to determine the best-fitting model to the experimental data:

$$r^2 = \frac{\sum \left(q_m - \overline{q_e} \right)^2}{\sum \left(q_m - \overline{q_e} \right)^2 + \sum \left(q_m - q_e \right)^2} \tag{1}$$

2. Materials and Methods

2.1. Materials

Fly ash precursor materials used in this study were obtained in Harare, Zimbabwe from a thermal power station firing bituminous coal. Random sampling was employed in obtaining the FA samples which were stored in air-tight containers. Collected FA samples had 20% unburnt carbon content, herein referred to as 20–FA. A portion of the FA was calcined in a muffle furnace at 905 °C for 2 hours to remove the unburnt carbon to achieve 0–FA samples. NaOH and hydrochloric acid (32%) were obtained from J.T. Baker chemical company. Chemical analysis of precursor materials and zeolite products were performed on a PANalytical Zetium X-ray Fluorescence (XRF) spectrometer, Netherlands. Metal ion determination was conducted on a Varian Spectr 20 plus atomic absorption spectrophotometer (AAS), Palo Alto, California, USA. Powder X-ray diffraction (PXRD) measurements were recorded on a powder D8 Advanced Powder X-Ray Diffractometer from Bruker Inc. (Karlsruhe, Germany) using Cu Kα (λ =1.54 Å) radiation source.

2.2. Zeolites Synthesis

The fusion method was used in this study as it has been shown to give a higher level of zeolitisation compared to the hydrothermal process [31]. The approach involved separately treating 50 g of the precursor materials (0-FA and 20-FA) with 250 mL of concentrated HCl under continuous agitation for 1 hour. The slurry obtained was filtered and the residue washed with deionized (DI) water until a neutral filtrate was obtained. Following acid treatments, 48 g of the precursor materials were crushed with 40 g of NaOH (ratio of 1.2:1) to form a homogeneous powder. The targeted ratio of 1.2:1 FA / NaOH has been shown to produce zeolites with high crystallinity and high CEC values [31–33]. The resulting powder was then fused in a muffle furnace at 550 °C for an hour followed by further grinding to get a homogeneous powder. 50 g of the fused samples were mixed with 100 mL of DI water, agitated continuously for 17 hours, and cured in an oven at 90 °C for six hours. The cured mixtures were filtered and the residue washed until the filtrate reached a pH of 8, followed by drying at 70 °C [31]. Zeolites obtained from 0-FA and 20-FA are herein referred to as Z-0 and Z-20 respectively and were stored in air tight containers until further analysis.
.

2.3. Cation Exchange Capacity Determination

Cation exchange capacities of all zeolite materials produced were determined in duplicates at pH 7. The ammonium acetate method was used at room temperature and it entailed mixing 5 g of the zeolites with 25 mL of 1 M ammonium acetate solution. The mixtures were then shaken for specified time periods ranging from 10 minutes to 18 hours to ascertain time for attainment of equilibrium. The reaction was quenched by centrifugation, supernatant was collected, and the residue was mixed with 75 mL of ethanol, shaken and centrifuged. The collected supernatants were combined for exchangeable cations determination using AAS.

2.4. Equilibrium and Kinetic Adsorption Studies

The batch process was employed in calcium ion adsorption studies. Adsorption isotherm studies were performed using 1.0 g of the zeolite and 50 mL of a 240, 500, 1000, 1500, 2000, and 2500 mg L^{-1} Ca^{2+} ion solution in screw-capped vials at 303 K. The containers were shaken in a reciprocating water bath at 150 rpm for 80 minutes. After shaking, the mixtures were filtered, and the filtrates were measured for calcium ion concentration using AAS. The amount of Ca^{2+} ions adsorbed was determined and the adsorption capacity, q$_e$ (mg g^{-1}), was calculated according to equation 2.

$$q_e = \frac{V(C_0 - C_e)}{W} \tag{2}$$

where C_0 is the initial calcium ions concentration (mg L^{-1}), C_e is the equilibrium concentration, W is the mass of zeolites (g) and V is the volume of the solution (L). The data collected was used for adsorption isotherm model fitting using the Langmuir, Freundlich, Temkin, and Dubinin-Radushkevich isotherms. Kinetic studies were conducted using 1g of the zeolites and 50 mL of a 2000 ppm Ca^{2+} solution. The contact time ranged from 10 to 80 minutes. The amount of calcium ions removed was measured after each time interval. All analyses were performed in duplicate.

3. Results and discussion
3.1. Physicochemical Characterization
3.1.1. Mineralogical Characterization

Chemical analysis results from XRF show that FA's dominant components are silica (55.76%), alumina (27.92%), calcium oxide (4.96%) and oxides of iron (3.5%) (hematite (Fe_2O_3) and magnetite (Fe_3O_4)) as shown in Table 1 (see Figure 1 for the corresponding XRD traces). The chemical composition of FA has been shown to depend largely on the type of combusted coal, additives and the combustion technology [14]. XRF results indicates the acquired FA to be ASTM C 618 class F, consistent with FA obtained from the combustion of bituminous coal. The total sum of SiO_2, Al_2O_3 and Fe_2O_3 (87.20%) exceeded 70%, while CaO content (4.96%) did not exceed 20% (Table 1), in agreement with literature data for class F FA. Acid treatment resulted in little changes in alumina and silica content but a 40% reduction in iron was observed. Acid treatment has been shown to significantly reduce CaO and Fe_2O_3 while maintaining SiO_2 and Al_2O_3 levels [16] leading to increases in the composition of these oxides, especially SiO_2. The acid treatment stage increases FA's reactivity as well as the acidity of produced zeolite.

Table 1: Chemical composition of calcined FA and zeolites produced from different precursor materials.

SAMPLE	SiO₂ (%)	Al₂O₃ (%)	Fe₂O₃ (%)	Na₂O (%)	K₂O (%)	CaO (%)	MgO (%)	P₂O₅ (%)	MnO (%)	TiO (%)	BaO (%)	SO₃ (%)	CrO₃ (%)	Si/Al
F.A	55.76	27.92	3.52	1.36	0.40	4.96	1.84	0.31	0.075	1.16	0.011	1.24	0.102	1.99
Z-0	46.95	23.47	1.89	13.98	0.36	4.26	1.34	0.30	0.021	1.07	0.000	0.14	0.092	2.00
Z-20	36.14	16.57	1.09	8.78	0.25	1.80	0.85	0.01	0.032	1.12	0.034	1.07	0.033	1.81

In addition to FA's chemical composition (particularly the Si/Al ratio) that has been shown to play a key role in the type of zeolites produced [16], the synthetic method determines the nature in which the alkali activator interacts with the FA resulting in differences in the type and hence properties of zeolites synthesized [34]. The chemical composition shown in Table 1 indicates that the FA has a low Si/Al ratio (< 5) which favors the production of low-silica zeolites, e.g of the faujasite and linde groups [34]. There was a marked increase in the percentage of Na_2O in the zeolite materials, 14 and 9% for Z-0 and Z-20 respectively compared to the precursor material (1%). This sodium enrichment is due to Na$^+$ ions from the NaOH used in the alkaline fusion step that serve to balance the negative charge created during fusion treatment of zeolite synthesis [35].

Figure 1: XRD profiles of FA (a) and zeolite products, Z-20 (b) and Z-0 (c).

The XRD profiles shown in Figure 1 indicate the major mineral phases in FA to be mullite ($Al_6Si_2O_{13}$), quartz (SiO_2), hematite (Fe_2O_3) and magnetite (Fe_3O_4). The results are consistent with XRF analysis confirming alumina, silica, and iron as the major components of the fly ash and zeolites samples, in agreement with other FA produced from subbituminous coal [36, 37]. Figure 1also shows that both Z-0 and Z-20 are mixtures of Na-Y, Na-A, and hydroxysodalite ($Na_4Al_3Si_3O_{12}OH$) zeolites, with Z-0 also having significant amounts of Na-X zeolite. A higher degree of supersaturation has been shown to favor the formation of zeolite X, a metastable phase, that later recrystallizes to form the more stable hydroxysodalite (HS) zeolite. In our case, zeolite X partially transformed to the HS phase resulting in the coexistence of the two phases. Zeolites A and X have been reported to co-crystallize as two phases at 90 °C [34], while under certain conditions hydroxysodalite can be formed in addition to zeolites A and X. Single phases can, however, be formed by careful control of reaction conditions [38]. The effect of acid pretreatment of FA is observed from the absence of calcite from the treated FA and the synthesized zeolites.

3.1.2. Cationic Exchange Capacity

Exchange reactions using NH_4^+ ions as the exchange ions showed that exchangeable ions present in appreciable quantities in both Z-0 and Z-20 were Na^+, Ca^{2+}, Mg^{2+} and K^+ ions. The CEC of zeolites depend on the porosity and exchangeable cations within the zeolite structure. The CEC results of the prepared zeolites were calculated to be 560.2 and 444.2 meq/100g for Z-0 and Z-20 respectively. Hydroxysodalite has been shown to have a low CEC, hence affected the overall value for all the products [38]. The low CEC

of Z-20 stems from unburnt carbon depositing on particles' surfaces. This influences the effectiveness of the reaction between NaOH and FA during the fusion stage, which is critical in the synthesis of high CEC zeolites [39]. The obtained results are consistent with literature data reporting that CEC values depend strongly on the type of zeolites, with zeolite X having higher CEC than zeolite A [31]. Z-0 has a greater proportion of zeolite X compared to Z-20 and hence the observed higher CEC of the former. Sodium ions release profile shown in Figure S1 (supplementary materials) highlights clearly differences in the release rates of the two materials. Release from Z-0 was faster than Z-20 with equilibrium being attained after 30 minutes in Z-0 compared to around 60 minutes for Z-20. The slower rate of releasing Na$^+$ may be a result of carbon particles surrounding the zeolite particles hence creating mass transfer resistance.
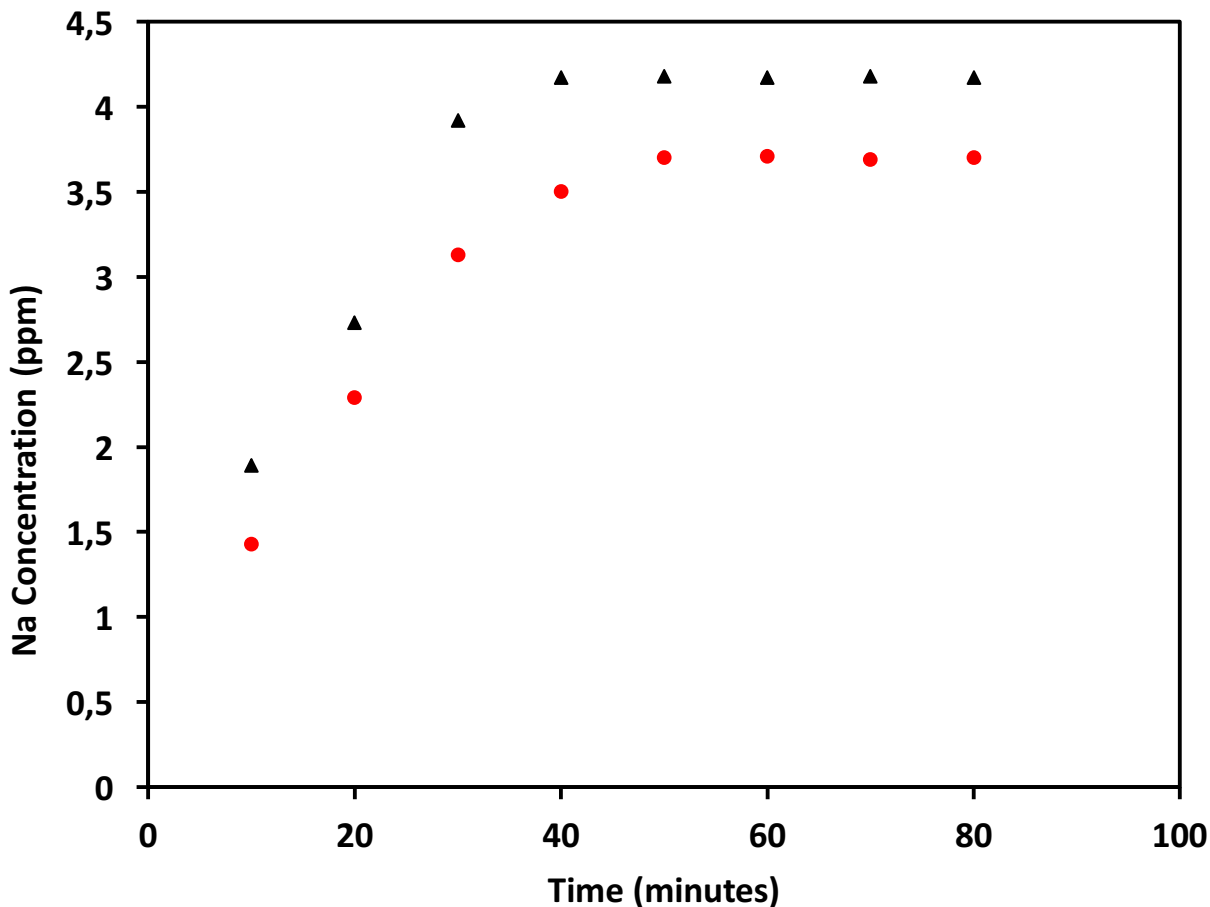
Figure S1: Time-dependent release of sodium ions from Z-0 (closed triangles) and Z-20 (closed circles).

3.2. Calcium Immobilisation
3.2.1. Effect of Dosage

The effects of adsorbent dosage on calcium ion adsorption by zeolites produced from both precursors are presented in Figure 2. Pollutant uptake from solution by adsorbents increases with the increase in adsorbent concentration due to the increase in the number of active sites available for adsorption. However, the enhancement effect is limited by an optimum value after which the uptake becomes constant (Figure 2a). At loadings below the optimum value, the adsorbent surfaces are easily saturated by the pollutant metal ions resulting in a low uptake of the ions from solution [40].
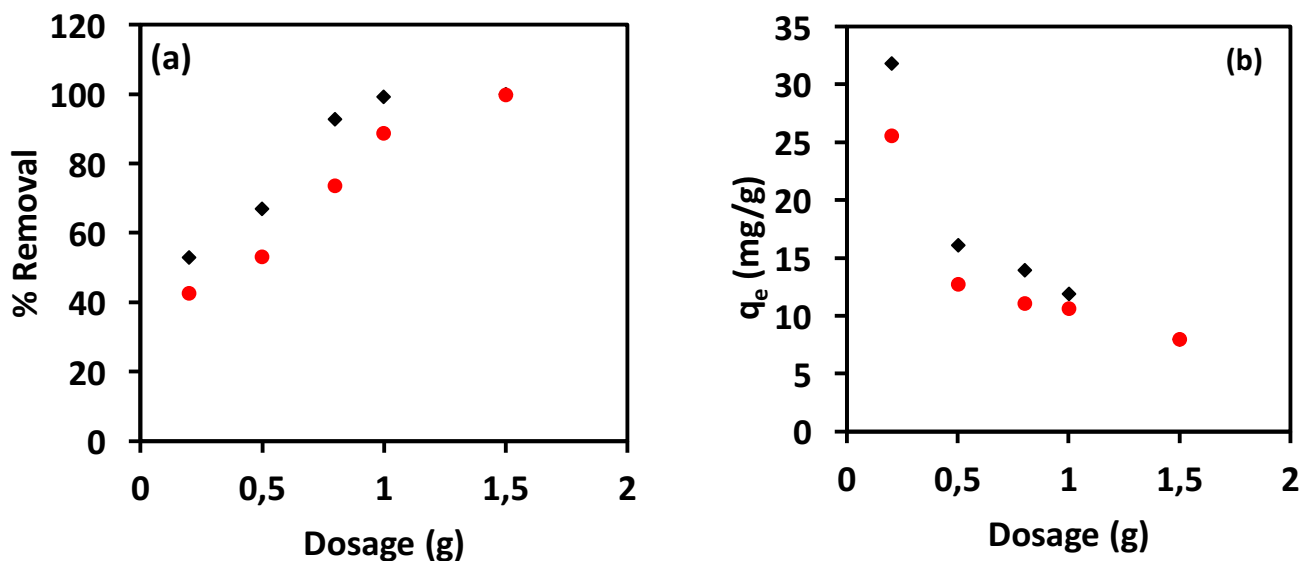
Figure 2: Effect of adsorbent dosage on Ca^{2+} ions adsorption by Z-0 (closed diamonds) and Z-20 (closed circles); (a) % removal (b) adsorption capacity, q_e. (T = 303 K, C_0 = 240 ppm, t = 150 minutes)

Incremental removal of Ca^{2+} ions becomes small towards equilibrium as the surfaces get saturated. Results from Figure 2a indicates optimum loadings for Z-0 and Z-20 to be 1.0 and 1.5 g respectively, all at 100% removal. However, removal efficiency as determined by adsorption capacity (mg g^{-1}) may vary as a function of the adsorbent loading, and the appearance of the graph generally depends on the adsorbent and the adsorbate (Figure 2b). Increasing adsorbent dose reduces the adsorption capacity due to overlapping of exchangeable sites, an effect of overcrowding adsorbent particles [30, 39]. Removal efficiencies shown in Figure 2b decrease continuously from the adsorbent loading of 0.1 to 1.5 g where 100% removal of Ca^{2+} ions was observed. Removal efficiency of Z-0 is higher than that of Z-20 at all loading levels except at 1.5 g where there is 100% removal for both adsorbents. Absorbent loading of 1.0 g was adopted for further studies.

3.2.1. Kinetic Study

The time-dependent removal of calcium ions shown in Figure 3 indicates that there is an initial fast rate of Ca^{2+} ions removal from solution for both adsorbent materials. A large number of available adsorption sites and high Ca^{2+} ion concentration in the bulk solution leads to a large driving force for adsorption (q_e-q_t) resulting in high adsorption rates during the early time regime (first 20 minutes). As the Ca^{2+} ion concentration in the bulk solution decrease, q_t increases and the driving force for the adsorption process and hence the reaction rate decrease until a quasi-equilibrium state is attained. Steady-state conditions were assumed, and a quasi-equilibrium state considered when adsorption capacity was almost constant, less than 1% difference in adsorption capacities in consecutive measurements (50 and 60 minutes). To better understand the time dependency of the adsorption process, kinetic studies involving the Lagergren [41], pseudo second order [42], and the Weber-Morris kinetic models were conducted and the results are summarized in Table 2 (linear fitting) and Table 3 (non-linear fitting). The Lagergren equation is also referred to as the pseudo first order (PFO) model to distinguish kinetic equations based on the adsorption

capacity of a solid from those based on the concentration of a solution [43]. The general non-linear equation (3) can be linearized into the widely used linear form (4).

$$q_t = q_e\left(1 - e^{-k_1 t}\right)$$ (3)

$$\log(q_e - q_t) = \log(q_e) - \frac{k_1}{2.303}t$$ (4)

where q_e and q_t (mg g^{-1}) are the adsorption capacities at equilibrium and at time t respectively, k_1 (min^{-1}) is the pseudo first order rate constant. The pseudo second order (PSO) rate equation was first applied in heavy metal adsorption by Ho et al. who successfully used it in the competitive removal of heavy metals by a biosorbent [42]. The modified model has found widespread usage and has general equations shown in equations 5 (non-linear) and 6 (linear).

$$q_t = \frac{k_2 q_e^2 t}{1 + k_2 q_e t}$$ (5)

$$\frac{t}{q_t} = \frac{1}{k_2 q_e^2} + \frac{t}{q_e}$$ (6)

where k_2 is the pseudo-second-order rate constant (g mg^{-1} min^{-1}). The intraparticle diffusion model, also known as the Weber-Morris model can be represented as:

$$q_t = k_{id} t^{0.5} + C$$ (7)

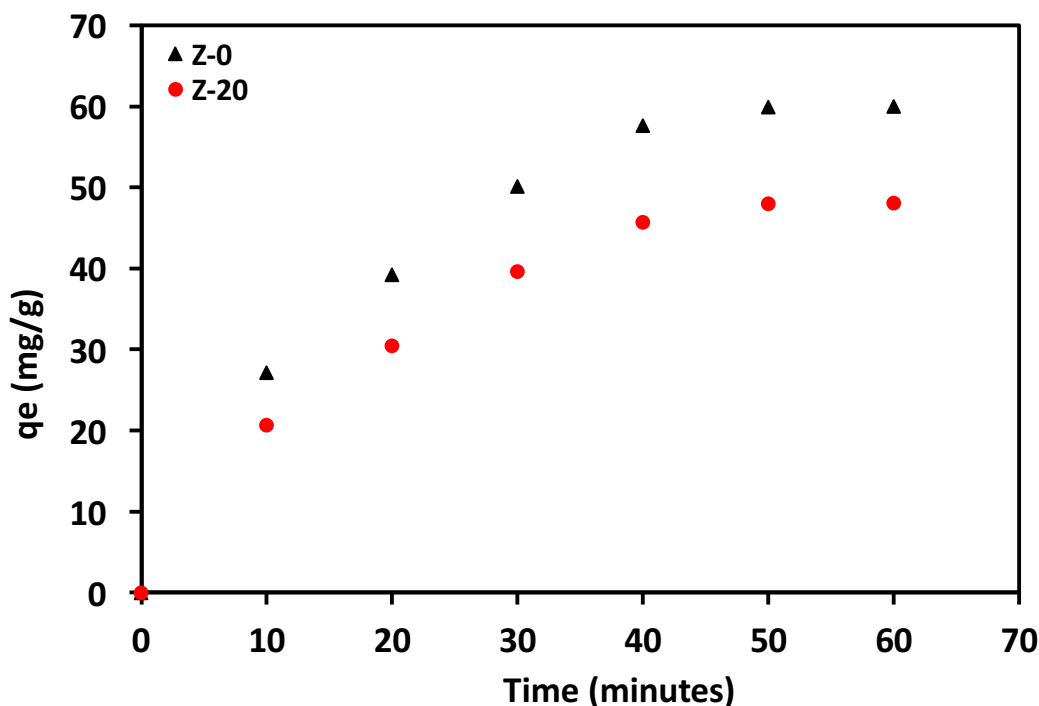with k_{id} being the intraparticle diffusion rate constant.

Figure 3: Time-dependent adsorption of Ca^{2+} ions onto Z-0 (closed triangles) and Z-20 (closed circles): T= 303 K, C$_o$ = 2000 ppm, pH = 7

Kinetic analysis results from linear regression analysis showed pseudo second order reaction model to be the best model in describing Ca^{2+} ions adsorption onto both Z-0 and Z-20 adsorbents (Figure 4 and Table

2). The kinetic analysis was achieved by considering the coefficient of determination (R^2) values for all models as well as adsorption capacities for PFO and PSO kinetic models. The PSO model has the highest R^2 values, 0.9847 and 0.9869 for Z-0 and Z-20 data respectively, and predicted q_e values were the closest to experimental values (Table 2). Linearized pseudo first order and Weber-Morris models showed poor fits to the experimental data. This shows that they are not applicable in describing the adsorption of Ca^{2+} ions onto the prepared zeolites, thus no further considerations of these models were undertaken. Rate constants obtained from the pseudo second order model are not significantly different, $(5 \pm 1_{.5}) \times 10^{-4}$ and $(6 \pm 1_{.8}) \times 10^{-4}$ g mg^{-1} g^{-1} for Z-0 and Z-20 respectively.
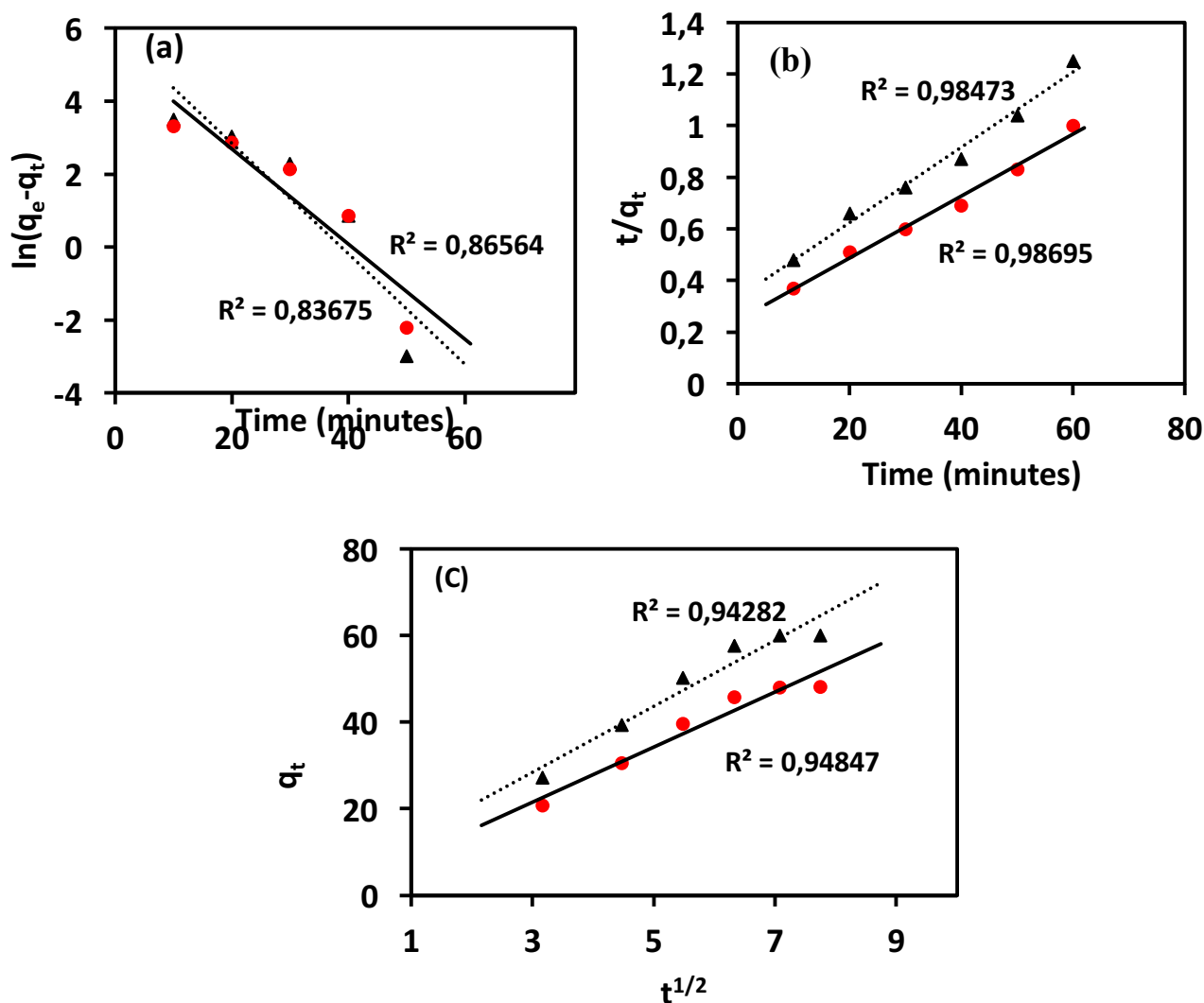
Figure 4: Linear fitting of Z-0 (closed triangles) and Z-20 (closed circles) to linear kinetic models, (a) pseudo-first-order model (b) pseudo-second-order model and (c) Webber-Morris model.

Results from non-linear curve fitting are shown in Figure 5 and parameters are summarized in Table 3. From Table 3, pseudo first order model has the highest R^2 value indicating a better fit when compared to pseudo second order and Weber-Morris models, consistent with graphs in Figure 5 which show that the best

fitting model to the experimental data is PFO. These results are at variance with linear fitting results (Table 2), which highlight the dangers of using linear regression to fit adsorption data. Table 3 also shows that non-linear PFO model predicts the q_e value more accurately when compared to the linearized form. Accordingly, results from non-linear curve fitting suggests the correct model to represent the kinetics of the adsorption process to be the pseudo first order model. This points to a linear dependence of the rate of adsorption on the driving force for the adsorption process [41, 43].

The large discrepancy between non-linear and linear goodness of fit of the pseudo first order equation highlights the error associated with the widely used linear curve fitting procedures. In this case, results from linear curve fitting erroneously indicated the adsorption process as following pseudo second order kinetics. This error can have great consequences in the optimization and design of adsorption systems as reaction kinetics play a great role in optimization and design processes. Another important result from this analysis is the close agreement between PSO results from linear fitting and non-linear fitting (Tables 2 and 3). The close agreements of the values of the rate constants and the predicted q_e values indicate that the linear form of the PSO used in this study, among other forms [45], is accurate in describing the kinetics process. Thus, the error in linear curve fitting analysis arise from linearization of the pseudo first order model. The rate constants obtained from PFO model in the non-linear analysis are $\left(5._2 \pm 1._1\right) \times 10^{-2}$ and $\left(4.8 \pm 0.7\right) \times 10^{-2} \, \text{min}^{-1}$ for the adsorption onto Z-0 and Z-20 respectively, also not significantly different.
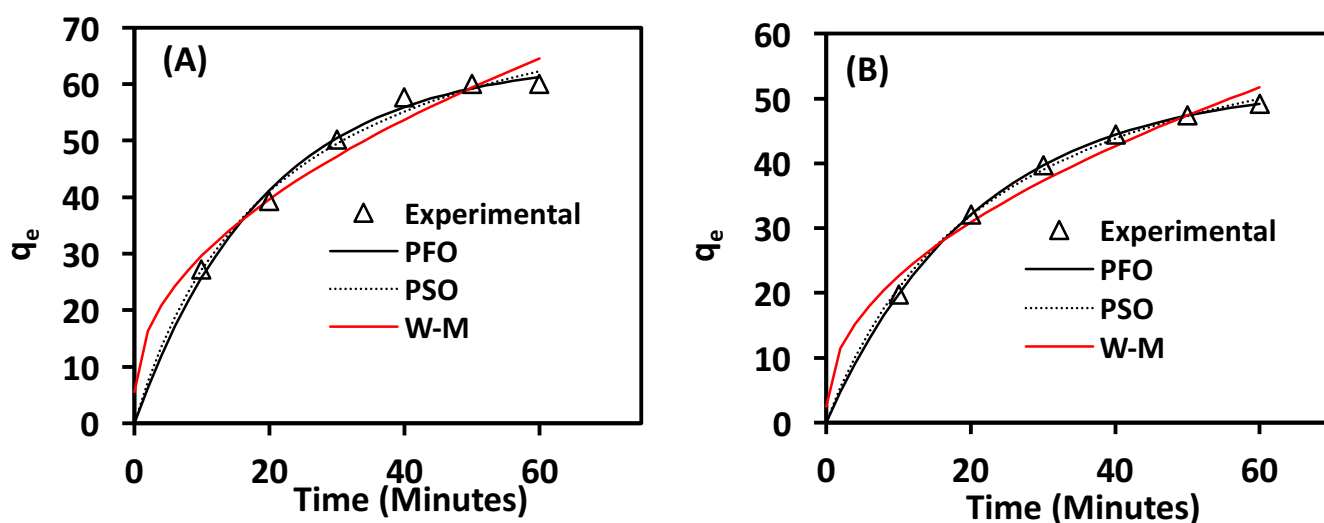

Figure 5: Non-linear fitting of Ca^{2+} ion adsorption to kinetic models (A) Z-0 and (B) Z-20.

3.2.3. Adsorption Isotherms

The capacity to gain a deep understanding of the adsorption mechanism enables optimization of the adsorption system's parameters which is essential for improving efficiency of the process for effective designing of adsorption systems. Fitting experimental data to adsorption isotherm models is the most widely used approach in determining the adsorption mechanism. In this study, common isotherm models viz. Langmuir, Freundlich, Temkin and Dubinin-Radushkevich (Table S1 in the supplementary materials) were applied to the experimental data. Curve fitting and hence extraction of adsorption parameters has routinely been done in two ways, non-linear and linear curve fitting. Linear fitting entails linearization of adsorption isotherms, a procedure that may results in errors in the obtained parameters.

Table 2: Summary of kinetic parameters for linear fitting of Ca^{2+} adsorption onto Z-0 and Z-20

Adsorbent	Pseudo first order model		Pseudo second order model			Weber-Morris	Experimental
	R^2	q_e (mg g^{-1})	k_2 (g g^{-1} min^{-1})	R^2	q_e (mg g^{-1})	R^2	q_e(mg g^{-1})
Z-0	0.8656	237	$(5 \pm 1._5) \times 10^{-4}$	0.9847	83	0.9428	74
Z-20	0.8368	202	$(6 \pm 1._8) \times 10^{-4}$	0.9869	69	0.9485	58

Table 3: Summary of kinetic parameters for non-linear fitting of Ca^{2+} adsorption onto Z-0 and Z-20

Adsorbent	Pseudo first order model			Pseudo second order model			Weber-Morris	Experimental
	R^2	q_e (mg g^{-1})	k_1 (min^{-1})	R^2	k_2 (g g^{-1} min^{-1})	q_e (mg g^{-1})	R^2	q_e(mg g^{-1})
Z-0	0.9881	64	$(5._1 \pm 1._5) \times 10^{-2}$	0.9825	$(5._7 \pm 1._5) \times 10^{-4}$	84	0.9431	74
Z-20	0.9944	52	$(4.8 \pm 1._5) \times 10^{-2}$	0.9885	$(6._1 \pm 1._8) \times 10^{-4}$	70	0.9642	58

Majoni and Masaya, J. Mater. Environ. Sci., 2020, 11(12), pp. 2034-2051

2044

For example, the Langmuir model can be linearized in four different ways (Table S1), all of which give different parameters. Linear fits of experimental data for Ca^{2+} ions adsorption to adsorption isotherms are summarized in Table S2 (supplementary materials). The coefficients of determination shown in Table S2 indicate the best fit to be Langmuir model linear form I (Langmuir I), $R^2 = 0.9975$ and 0.9921 for Ca^{2+} ions adsorption onto Z-0 and Z-20 respectively. Predicted q_m values from Langmuir I are also close to experimental q_e values indicating close fit of this linear form of the model to experimental data. The Langmuir model is consistent with the adsorption profiles shown in Figure 6 which indicates class (I) type adsorption, signifying chemical adsorption and monolayer coverage. Previously observed chemisorption of metal ions onto zeolites supports electrostatic attractions in which calcium ions replace exchangeable cations within the structures, mainly Na^+ and K^+ ions [44]. Non-linear fitting of the experimental data to adsorption isotherms results shown in Figure 7 and Table 4 indicate that the best model in describing the adsorption process is the Langmuir model. The Langmuir model has coefficient of determination values closest to 1 and q_m values that are close to experimental q_e values. Comparing Tables 4 & S2 shows that only Langmuir model linear form I has parameters close to parameters obtained from non-linear fitting. The results indicate that the linearization of the Langmuir model may introduce errors and there ought to be uttermost importance placed in choosing linear forms to apply in linear model fitting procedures. It is therefore advisable to use non-linear curve fitting to obtain accurate results.

Table S1: Adsorption isotherm models applied in this study

Model	Linear Equations	Parameters
Langmuir $$q_e =_L \frac{q_m K C_e}{1 + K_L C_e}$$	(i) $\dfrac{C_e}{q_e} = \dfrac{C_e}{q_m} + \dfrac{1}{q_m K_L}$ (ii) $\dfrac{1}{q_e} = \left[\dfrac{1}{q_m K_L}\right]\dfrac{1}{C_e} + \dfrac{1}{q_m}$ (iii) $q_e = q_m - \left[\dfrac{1}{K_L}\right]\dfrac{q_e}{C_e}$ (iv) $\dfrac{q_e}{C_e} = K_L q_m - K_L q_e$	q_m: maximum monolayer capacity, mg g^{-1} K_L: Langmuir constant q_e: amount adsorbed per unit weight of adsorbent, mg g^{-1} C_e: solute equilibrium concentration, mg L^{-1}
Freundlich $$q_e = K_F C_e^{1/n}$$	$\log(q_e) = \log K_F + \dfrac{1}{n}\log C_e$	K_F :adsorption capacity $1/n$: represents adsorption intensity
Temkin $$q_e = \frac{RT \ln(K_T C_e)}{b_T}$$	$q_e = \dfrac{RT}{b_T}\ln K_T + \left(\dfrac{RT}{b_T}\right)\ln C_e$	B: Temkin constant which is related to the heat of sorption K_T: Temkin isotherm constant, L g^{-1}
Dubinin-Radushkevich (D-R) $$q_e = q_s e^{-K_{DR}\varepsilon^2}$$	$\ln q_e = \ln(q_m) - B_D \varepsilon^2$: $\varepsilon = RT \ln\left[1 + \dfrac{1}{C_e}\right]; E = \dfrac{1}{\sqrt{2B_D}}$	B_D: Dubinin-Radushkevich constant related to energy. ε: Polanyi potential

Table S2. Summary of linear adsorption isotherm fitting parameters

Model			Adsorbent					
	Z-0				**Z-20**			
	R^2	q_m (mg/g)	Parameter	Experimental q_e (mgg^{-1})	R^2	q_m (mg/g)	Parameter	Experimental q_e (mgg^{-1})
Langmuir								
I	0.9975	63	0.023 (K_L)	74	0.9921	54	0.0059 (K_L)	58
II	0.8839	44	0.217 (K_L)	74	0.9322	43	0.0115 (K_L)	58
III	0.6005	50	0.177 (K_L)	74	0.7799	48	0.0094 (K_L)	58
IV	0.6005	55	0.106 (K_L)	74	0.7799	52	0.0073 (K_L)	58
Freundlich	0.9665	N/A	1.832 (K_F)	74	0.9503	N/A	2.5503 (K_F)	58
Temkin	0.9179	N/A	1.530 (K_T)	74	0.9354	N/A	0.008 (K_T)	58
D-R	0.6269	45	1.01×10^{-6} (B_D)	74	0.6230	37	1.59×10^{-4} (B_D)	58
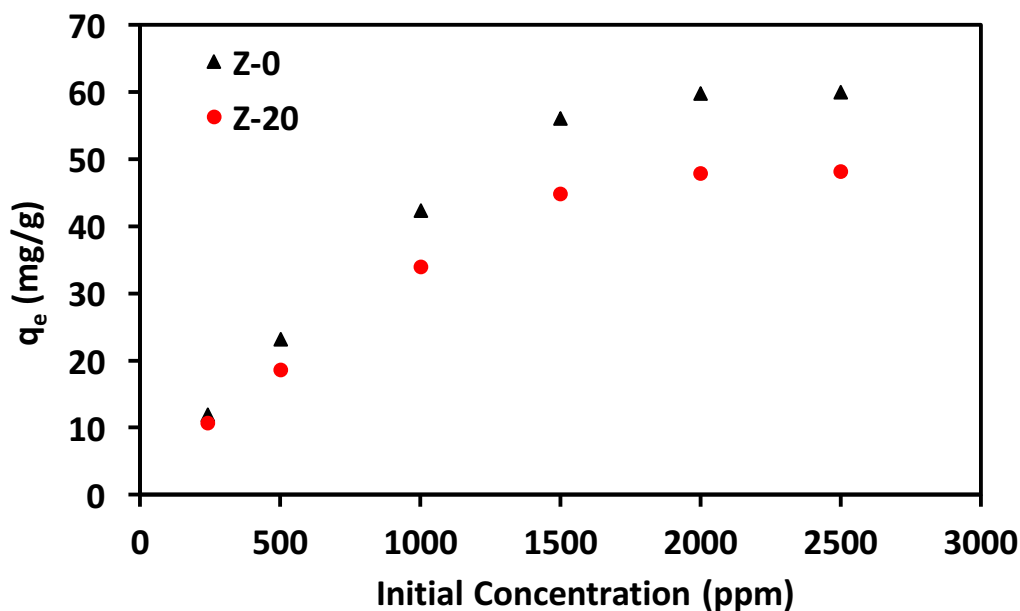
Figure 6: Effect of initial concentration on Ca^{2+} adsorption

While Langmuir I has been shown to be accurate in describing the adsorption system under investigation, other authors have found different linear forms to correctly represent their data sets [44,45]. The results indicate that if linear model fitting cannot be avoided, then it is recommended that all the Langmuir linear forms be tested to identify the one that correctly represent the adsorption system under investigation. Extreme caution need to be exercised though as Sahin and Tapadia's work highlights the dangers of reliance on coefficient of determination only as they identified the linear form (linear form IV) with predicted parameters close to those obtained from non-linear curve fitting had the lowest R^2 value [45].
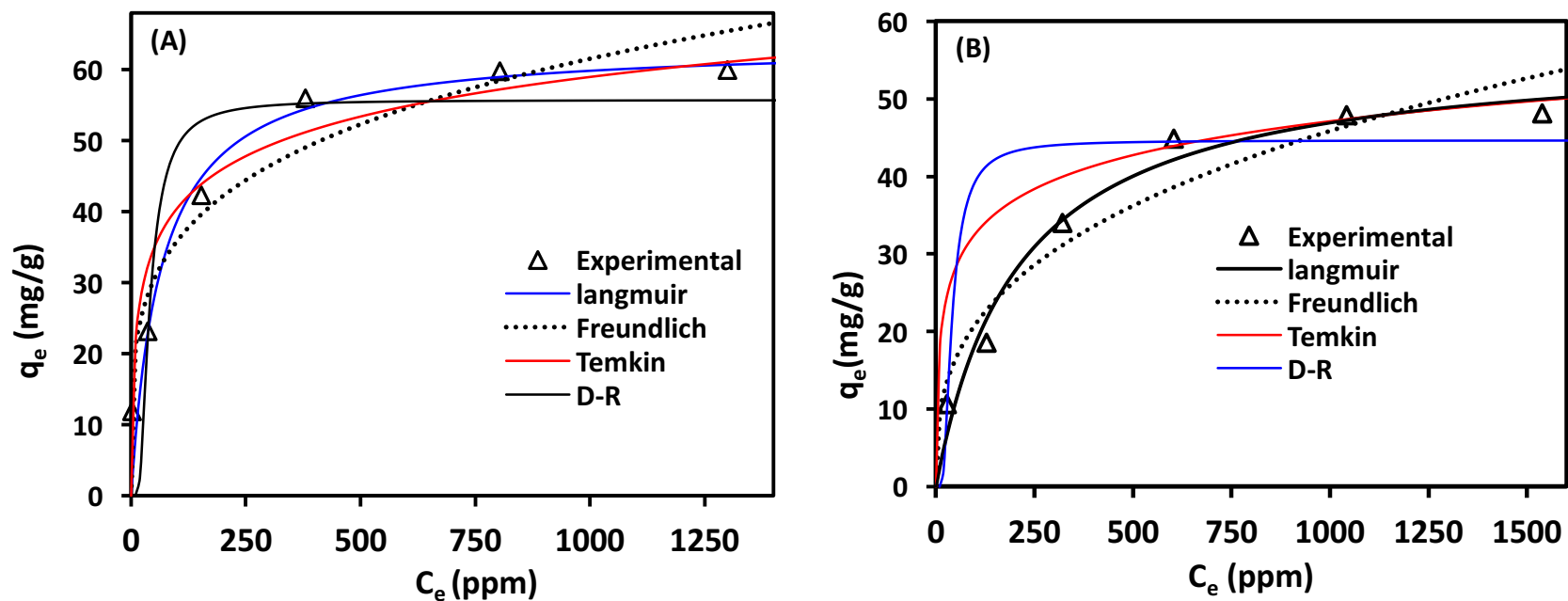
Fig. 7 Experimental data and non-linear fitting of adsorption isotherms for the adsorption of Ca^{2+} onto (a) Z-0 and (b) Z-20

Table 4: Summary of non-linear adsorption isotherm fitting parameters

Zeolite	Langmuir				Freundlich	Temkin	D-R	Experimental
	R^2	q_m (mg/g)	K_L	R_L	R^2	R^2	R^2	q_e (mg/g)
Z-0	0.9847	63.7	0.0254	0.78—0.30	0.9439	0.9349	0.8621	74
Z-20	0.9707	57.0	0.0048	0.84—0.34	0.9231	0.9264	0.8396	58

Majoni and Masaya,, J. Mater. Environ. Sci., 2020, 11(12), pp. 2034-2051

2047

Parameters from Langmuir isotherm show that Z-0 has a Langmuir constant value that is 5 times greater than that for Z-20 which indicates a much higher affinity for Ca^{2+} ions compared to Z-20. Even though the Langmuir constant value for C-20 was much less than that of Z-0, the adsorption capacity for Z-20 (57.0 mg g^{-1}) was only 20% less than that of Z-0 (63.7 mg g^{-1}), consistent with cation exchange capacity results. This indicates that fly ash with high unburnt carbon content can be used to prepare adsorbents that have high Ca^{2+} ion adsorption efficiency without the need for calcination thereby reducing production cost. One of the key features of the Langmuir isotherm is the dimensionless separation factor (R_L) which can be used to assess the adsorption process as unfavorable ($R_L > 1$), linear ($R_L = 1$), favorable ($0 < R_L < 1$) or irreversible ($R_L = 0$). The separation factor is defined by the following equation:

$$R_L = \frac{1}{1 + K_L C_0} \tag{8}$$

where C_0 (mg L^{-1}) is the initial adsorbate concentration. Separation factor analysis results (Figure S2 and Table 4) indicates separation factor values between zero and one at all the initial concentrations employed here, indicating favourable interactions between the zeolites and Ca^{2+} ions. The analysis also reveal that the reaction was more favourable at higher initial Ca^{2+} ions concentration, and the adsorption of Ca^{2+} ions onto Z-0 is more favourable than onto Z-20.
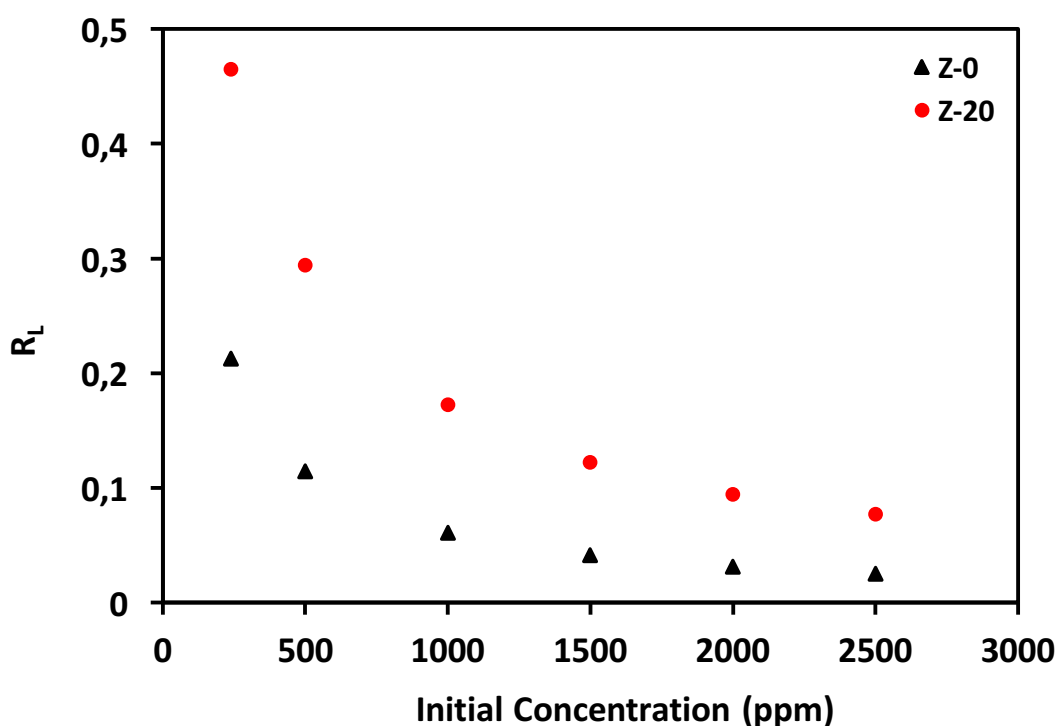

Figure S2. R_L values for adsorption of Ca^{2+} onto Z-0 (closed triangles) and Z-20 (closed circles).

Conclusion

Coal fly ash with a high unburnt carbon content was used to successfully synthesize an adsorbent material that was a mixture of zeolites A, Y and hydroxysodalite. Even though the adsorbent had an adsorption capacity 20% less than that prepared from calcined fly ash, it had high cationic exchange capacity and Ca^{2+} ions adsorption efficiency. Non-linear and linear model fitting procedures conducted indicated that it is inappropriate to use the linear form of the Lagergren (pseudo first order kinetic) expression to assess whether the experimental data follow first order kinetics. Therefore, the use of non-linear curve fitting is highly recommended when checking the applicability of pseudo first order model

in describing the adsorption kinetics. Non-linear model fitting of experimental data to kinetic models and adsorption isotherms revealed that the adsorption process follows first order kinetics and is well described by the Langmuir adsorption isotherm. The Langmuir separation factor indicated that the adsorption of Ca^{2+} ions on both adsorbents was favourable. The study showed that an efficient adsorbent that can be utilized in water softening can be produced from fly ash with high unburnt carbon content without the need of the energy intensive high temperature calcination process.

References

[1] U. S. Energy Information Administration's International Energy Outlook 2020, *Https://Www.Eia.Gov/Outlooks/Ieo/*, vol. 2020 Available: https://www.eia.gov/outlooks/ieo/.

[2] I. Pappis, M. Howells, V. Sridharan, W. Usher, A. Shivakumar, F. Gardumi, E. Ramos, Energy projections for African countries, Hidalgo Gonzalez, I., Medarac, H., Gonzalez Sanchez, M. and Kougias, I., editor(s), EUR 29904 EN. doi: 10.2760/678700.

[3] "Eskom and ash management," *Eskom and ash management*, 2016. http://www.eskom.co.za/news/Pages/Feb20.aspx (accessed Dec. 28, 2020).

[4] Y.W. Go, S.H. Yeom, Fabrication of a solid catalyst using coal fly ash and its utilization for producing biodiesel, *Environ. Eng. Res.* 24 (2019) 324–330. doi: 10.4491/EER.2018.029.

[5] S.K. Patel, H.P. Satpathy, A.N. Nayak, C.R. Mohanty, Utilization of Fly Ash Cenosphere for Production of Sustainable Lightweight Concrete, *J. Inst. Eng. Ser. A.* 101 (2020) 179–194. doi: 10.1007/s40030-019-00415-6.

[6] N. Ghazali, K. Muthusamy, S. Wan Ahmad, Utilization of Fly Ash in Construction, *IIOP Conf. Ser. Mater. Sci. Eng.* 601, no. 012023, 2019, doi: 10.1088/1757-899X/601/1/012023.

[7] N. Czuma, P. Baran, W. Franus, P. Zabierowski, K. Zarębska, Synthesis of zeolites from fly ash with the use of modified two-step hydrothermal method and preliminary SO_2 sorption tests, *Adsorpt. Sci. Technol.* 37 (2019) 61–76. doi: 10.1177/0263617418810607.

[8] "Fly ash geopolymer concrete: Significantly enhanced resistance to extreme alkali attack (2020, May 7) retrieved 27 December 2020 from https://phys.org/news/2020-05-ash-geopolymer-concrete-significantly-resistance.html."

[9] A. Naghizadeh, S.O. Ekolu, I. Musonda, High temperature heat - Treatment (HTHT) for partial mitigation of alkali attack in hardened fly ash geopolymer binders, *Case Stud. Constr. Mater.* 12 (2020) e00341. doi: 10.1016/j.cscm.2020.e00341.

[10] S. Gorai, Utilization of Fly ash for sustainable environment management, *J. Mater. Environ. Sci.* 9 (2018) 385–393.

[11] S. Boycheva *et al.*, "Progress in the utilization of coal fly ash by conversion to zeolites with green energy applications," *Materials (Basel).* 13 (2020). doi: 10.3390/MA13092014.

[12] M E. Davis, R.F. Lobo, Zeolite and Molecular Sieve Synthesis, *Chem. Mater.* 4 (1992) 756–768.

[13] C. Amrhein, H. Gholam, T.S. Kim, P.A. Mosher, R. Gagajena, T. Amanios, L.D.E.L.A. Torre, Synthesis and Properties of Zeolites from Coal Fly Ash, *Environ. Sci. Technol.* 30 (1996) 735–742. doi:10.1021/es940482c.

[14] A. Bhatt, S. Priyadarshini, A. M. Aiswarya, A. Abri, M. Sattler, S. Techapaphawit, Physical, chemical, and geotechnical properties of coal fly ash: A global review, *Case Stud. Constr. Mater.* 11, (2019) e00263. doi: 10.1016/j.cscm.2019.e00263.

[15] S.S. Bukhari, J. Behin, H. Kazemian, S. Rohani, Conversion of coal fly ash to zeolite utilizing microwave and ultrasound energies: A review, *Fuel*. 140 (2015) 250–266. doi: 10.1016/j.fuel.2014.09.077.

[16] V. Volli, M.K. Purkait, Selective preparation of zeolite X and A from flyash and its use as catalyst for biodiesel production, *J. Hazard. Mater.* 297 (2015) 101–111. doi:10.1016/j.jhazmat.2015.04.066.

[17] T. Aldahri, J. Behin, H. Kazemian, S. Rohani, Synthesis of zeolite Na-P from coal fly ash by thermo-sonochemical treatment, *Fuel*l. 182 (2016) 494–501. doi: 10.1016/j.fuel.2016.06.019.

[18] Z. Liu, C. Shi, D. Wu, S. He, B. Ren, A Simple Method of Preparation of High Silica Zeolite Y and Its Performance in the Catalytic Cracking of Cumene, *J. Nanotechnol.* (2016) Article ID 1486107. doi.org/10.1155/2016/1486107

[19] T. Henmi, Increase in Cation Exchange Capacity of Coal Fly Ash by Alkali Treatment, *Clay Sci.* 282 (1987) 277–282.

[20] X. Ren *et al.*, Synthesis of zeolites from coal fly ash for the removal of harmful gaseous pollutants: A review, *Aerosol Air Qual. Res.* 20 (2020) 1127–1144. doi: 10.4209/aaqr.2019.12.0651.

[21] J.L.X. Hong, T.Maneerung, S.N. Koh, S. Kawi, C.H. Wang, Conversion of Coal Fly Ash into Zeolite Materials: Synthesis and Characterizations, Process Design, and Its Cost-Benefit Analysis, *Ind. Eng. Chem. Res.* 56 (2017) 11565–11574. doi: 10.1021/acs.iecr.7b02885.

[22] O.D. Ozdemir, S. Piskin, A Novel Synthesis Method of Zeolite X From Coal Fly Ash: Alkaline Fusion Followed by Ultrasonic-Assisted Synthesis Method," *Waste and Biomass Valorization*. 10 (2019) 143–154. doi: 10.1007/s12649-017-0050-7.

[23] B. Rubio, M.T. Izquierdo, M.C. Mayoral, M.T. Bona, M.J. Andres, Unburnt carbon from coal fly ashes as a precursor of activated carbon for nitric oxide removal, *J. Hazard. Mater.* 143 (2007) 561–566.

[24] C.P. Valderrama, J.T. Agredo, R.M. Gutierrez, A high unburned carbon fly ash concrete's performance characteristics, *Ing. E Investig.* 31 (2011) 39–46.

[25] P. Hamley, E. Lester, A. Thompson, M. Cloke, M. Poliakoff, The removal of carbon from fly ash using supercritical water oxidation, in: 2001 Int. Ash Util. Symp. Cent. Appl. Energy Res. Univ. Kentucky, 2001.

[26] G. Li, L. Deng, J. Liu, Y. Cao, H. Zhang, J. Ran, A New Technique for Removing Unburned Carbon from Coal Fly Ash at an Industrial Scale, *Int. J. Coal Prep. Util.* 35 (2015) 273–279. doi:10.1080/19392699.2015.1008098.

[27] H. Sung, K. Yoo, S. Lee, The removal of unburned carbon from fly ash by kerosene extraction, *Geosystem Eng.* 9328 (2016) 1–4. doi:10.1080/12269328.2015.1096841.

[28] J. Kim, H. Cho, S. Kim, Removal of Unburnt Carbon from Coal Fly Ash Using a Pneumatic Triboelectrostatic Separator, *J. Environ. Sci. Heal. Part A.* 36 (2001) 1709–1724. doi:10.1081/ESE-100106253.

[29] A. Walker, T.D. Wheelock, Separation of Carbon from Fly Ash Using Froth Flotation, *Coal Prep.* 26 (2006) 235–250. doi:10.1080/07349340601104883.

[30] D.P. Mishra, S.K. Das, A study of physico-chemical and mineralogical properties of Talcher coal fly ash for stowing in underground coal mines, *Mater. Charact.* 61 (2010) 1252–1259. doi:10.1016/j.matchar.2010.08.008.

[31] A. Molina, C. Poole, A comparative study using two methods to produce zeolites from fly ash, *Miner. Eng.* 17 (2004) 167–173.

[32] K. Ojha, N.C. Pradhan, A.N. Samanta, Zeolite from fly ash : synthesis and characterization, *Bull. Mater. Sci.* 27 (2004) 555–564.

[33] Y. Zhang, J. Dong, F. Guo, Z. Shao, J. Wu, Zeolite Synthesized from Coal Fly Ash Produced by a Gasification process for Ni^{2+} Removal from Water, *Minerals.* 8 (2018) 1–14. doi:10.3390/min8030116.

[34] S. Singh, L.C. Ram, R.E. Masto, S.K. Verma, A comparative evaluation of minerals and trace elements in the ashes from lignite, coal refuse, and biomass fired power plants, *Int. J. Coal Geol.* 87 (2011) 112–120. doi:10.1016/j.coal.2011.05.006.

[35] V.K. Jha, M. Nagae, M. Matsuda, M. Miyake, Zeolite formation from coal fly ash and heavy metal ion removal characteristics of thus-obtained Zeolite X in multi-metal systems, *J. Environ. Manage.* 90 (2009) 2507–2514.

[36] M. Zyrkowski, R.C. Neto, L.F. Santos, K. Witkowski, Characterization of fly-ash cenospheres from coal-fired power plant unit, *Fuel.* 174 (2016) 49–53. doi:10.1016/j.fuel.2016.01.061.

[37] R.T. Chancey, P. Stutzman, M.C.G. Juenger, D.W. Fowler, Comprehensive phase characterization of crystalline and amorphous phases of a Class F fly ash, *Cem. Concr. Res.* 40 (2010) 146–156. doi:10.1016/j.cemconres.2009.08.029

[38] D. Wu, B. Zhang, L. Yan, H. Kong, X. Wang, Effect of some additives on synthesis of zeolite from coal fly ash, *Int. J. Miner. Process.* 80 (2006) 266–272. doi:10.1016/j.minpro.2006.05.005.

[39] A.M. Cardoso, A. Paprocki, L.S. Ferret, C.M.N. Azevedo, M. Pires, Synthesis of zeolite Na-P1 under mild conditions using Brazilian coal fly ash and its application in wastewater treatment, *Fuel.* 139 (2015) 59–67. doi:10.1016/j.fuel.2014.08.016.

[40] C.H.S. Gulipalli, B. Prasad, K.L. Wasewar, Batch Study, Equilibrium and Kinetics of Adsorption of Selenium Using Rice Husk Ash (RHA), *J. Eng. Sci. Technol.* 6 (2011) 586–605.

[41] S. Lagergren, About the theory of so-called adsorption of soluble substances, *K. Sven. Vetenskapsakad.* Handl., Band 24 (1898) 1–39.

[42] Y.S. Ho, D.A.J. Wase, C.F. Forster, Kinetic Studies of Competitive Heavy Metal Adsorption by Sphagnum Moss Peat, *Environ. Technol.* 17 (1996) 71–77. doi:10.1080/09593331708616362.

[43] Y. Ho and G. McKay, , A Comparison of Chemisorption Kinetic Models Applied to Pollutant Removal on Various Sorbents, *Process Saf. Environ. Prot.* 76 (1998) 332–340.

[44] M. Visa, Synthesis and characterization of new zeolite materials obtained from fly ash for heavy metals removal in advanced wastewater treatment, *Powder Technol.* 294 (2016) 338–347. doi:10.1016/j.powtec.2016.02.019.

[45] R. Sahin, K. Tapadia, Comparison of linear and non-linear models for the adsorption of fluoride onto geo-material: limonite, *Water Sci. Technol.* 72 (2015) 2262–2269. doi:10.2166/wst.2015.449.

[46] S.-C. Tsai, K.-W. Juang, Comparison of Linear and Nonlinear Forms of Isotherm Models for Strontium Sorption on a Sodium Bentonite, *J. Radioanal. Nucl. Chem.* 243 (2000) 741–746.

(2020) ; http://www.jmaterenvironsci.com